AIAA JOURNAL
Vol. 46, No. 11, November 2008

Eigenmodes of a Counter-Rotating Vortex Dipole

Leo M. González, Rafael Gómez-Blanco, and Vassilis Theofilis*
Universidad Politécnica de Madrid, 28040 Madrid, Spain

DOI: 10.2514/1.35511

Highly resolved solutions of the two-dimensional incompressible Navier–Stokes and continuity equations describing the evolution of a counter-rotating pair of vortices have been obtained accurately and efficiently by spectral-collocation methods and an eigenvalue decomposition algorithm. Such solutions have formed the basic state for subsequent three-dimensional biglobal-eigenvalue-problem linear-instability analyses, which monitor the modal response of these vortical systems to small-amplitude perturbations, periodic along the homogeneous axial spatial direction, without the need to invoke an assumption of azimuthal spatial homogeneity. A finite element methodology (González, L. M., Theofilis, V., and Gomez-Blanco, R., "Finite Element Numerical Methods for Viscous Incompressible Biglobal Linear Instability Analysis on Unstructured Meshes," *AIAA Journal*, Vol. 45, No. 4, 2007, pp. 840–855) has been adapted to study the instability of vortical flows and has been validated on the Batchelor vortex (Mayer, E. W., and Powell, K. G., "Viscous and Inviscid Instabilities of a Trailing Vortex," *Journal of Fluid Mechanics*, Vol. 245, 1992, pp. 91–114). Subsequently, the instability of the counter-rotating dipole has been analyzed; aspects monitored have been the dependence of the results on the Reynolds number, the value of the (nonzero) axial velocity considered, and the time at which the quasi-steady basic flow has been monitored. Essential to the success of the analysis has been the appropriate design of a calculation mesh, as well as exploitation of the symmetries of the basic state. The spatial structure of the amplitude functions of all unstable eigenmodes reflects the inhomogeneity of the basic state in the azimuthal spatial direction, thus providing a posteriori justification for the use of the biglobal-eigenvalue-problem concept.

Nomenclature

a, a_0	=	vortex radius, initial vortex radius
a_{th}	=	theoretical vortex radius
a_y, a_z	=	vorticity polar moments
b, b_0	=	distance between vortices, initial distance between vortices
$\mathcal{D}_y$, $\mathcal{D}_z$	=	Fourier spectral-collocation differentiation matrices in the y and z spatial directions
E	=	vortex aspect ratio
L_x	=	periodicity length in the x direction
m	=	Krylov subspace dimension
N	=	number of quadratic (velocity) nodes
NL	=	number of linear (pressure) nodes
N_y, N_z	=	number of Fourier spectral-collocation points in the y and z spatial directions
p	=	pressure
Re	=	Reynolds number
r	=	radial coordinate
t	=	nondimensional time
t^*	=	dimensional time
U_0	=	axial velocity parameter
u_i	=	fluid velocity component
x_i	=	spatial coordinates
y_c, z_c	=	y and z coordinates of vorticity centroids
y_∞, z_∞	=	domain limits for the basic flow calculation
α	=	wave-number parameter ($2\pi/L_x$)
Γ, Γ_0	=	circulation, initial circulation
ε	=	parameter $\ll 1$
ζ	=	vorticity
ν	=	kinematic viscosity
ψ	=	stream function
ω_i	=	amplification/damping rate of linear perturbations ($\equiv \Re\{\omega\}$)
ω_r	=	perturbation frequency ($\equiv \Im\{\omega\}$)
$\bar{}$	=	basic flow component
$\hat{}$	=	amplitude function
$\tilde{}$	=	perturbation component

Presented as Paper 4539 at the 37th AIAA Fluid Dynamics Conference and Exhibit, Miami, FL, 25–28 June 2007; received 7 November 2007; revision received 1 April 2008; accepted for publication 1 April 2008.

*School of Aeronautics; vassilis@aero.upm.es. Corresponding Author.

I. Introduction

WORK spanning several decades exists that focuses on the problem of inviscid or viscous instability of vortical flows. Short of resorting to a direct numerical simulation methodology analysis [1], an approach hardly appropriate for parametric studies, practically all instability work has dealt with basic flows that correspond to vortices either in isolation or in the presence of a shear flow that models the presence of a second co- or counter-rotating vortex. In contrast, Hein and Theofilis [2] and Jacquin et al. [3] first employed the biglobal-instability-analysis concept [4] to analyze three-dimensional instability of arbitrary vorticity distributions on the plane normal to the axial direction, treating the latter spatial direction as homogeneous, but without resorting to the assumption of spatial homogeneity in the azimuthal direction. The basic states analyzed in those works were constructed analytically with the aid of the Batchelor-vortex model. Interestingly, validation studies on the Batchelor vortex [2] demonstrated the stringent resolution requirements placed on the stability analysis by the tight structure of the amplitude functions of the small-amplitude perturbations developing in the core of the basic flow vortex. The use of a regular Cartesian tensor-product spectral-collocation computational mesh [2] has adversely influenced the convergence of the results presented (though convergence has been achieved), because a large portion of the available (mapped) Chebyshev collocation points used have been wasted in resolving the innocuous far field.

It thus becomes natural to depart from the structured-mesh technologies used in the earlier analyses and to focus on numerical methodologies for biglobal instability analysis that rely on unstructured meshes. The work of Broadhurst et al. [5] was the first step in this direction, employing a spectral-hp element methodology. Building upon earlier work by González et al. [6], attention here is turned to a (standard Taylor–Hood element-based) finite element method (FEM) approach for the solution of the

incompressible biglobal eigenvalue problem (EVP). To eliminate potential influences of the basic state on the quality of the instability results, two-dimensional direct numerical simulation, based on spectral collocation and an eigenvalue decomposition algorithm, has been employed to obtain the basic state [7]. Results delivered by this methodology, when the direct numerical simulation (DNS) is initialized on different models of aircraft wing loading, have been found to be in excellent agreement with those produced by a different, appropriate, and efficient DNS methodology for problems of this class [1,8].

Here, the initial conditions are provided by a counter-rotating pair of vortices; after an initial transient period, a dipole is formed that descends and diffuses according to the imposed Reynolds number. Photographs in time of this flowfield are extracted at predefined characteristic times [9] and are analyzed with respect to their three-dimensional instability. Turning to the biglobal EVP, the present FEM-based methodology has been validated against instability results of a single-Batchelor vortex [10]. This exercise has delivered information regarding efficient meshing strategies and resolution requirements for in-core serial solution of the EVP. This knowledge, in addition to appropriate boundary conditions, motivated by the symmetries of the basic state, has then been applied to the numerically defined vortex dipole problem.

Section II discusses the theoretical background of both the basic flow and the eigenvalue problem, as well as the boundary conditions of the stability problem and aspects of the numerical solution of both basic and perturbed flows. Subsequently, results are presented in Sec. III on the instability of both the isolated Batchelor vortex and the numerically obtained dipoles. The three aspects monitored in the present multiparametric problem are 1) the dependence of the eigenspectrum on Reynolds number, 2) the effect of different values of the axial velocity on instability, and 3) the effect of diffusion expressed via different times at which the photographs of the basic flow is extracted from the DNS data. Conclusions and projected future directions of the present research are discussed in Sec. IV.

II. Theory

Starting from a variational formulation of the linearized Navier–Stokes equations around a base flow, a p-FEM discretization is performed using a Galerkin method, as follows. The equations governing incompressible flows are written in primitive-variable formulation, and steady nonparallel basic flows $(\bar{u}_i, \bar{p})^T$ are perturbed by small-amplitude velocity $\tilde{u}_i$ and kinematic pressure $\tilde{p}$ perturbations, as follows:

$$u_i = \bar{u}_i + \varepsilon\tilde{u}_i + \text{c.c.}, \qquad p = \bar{p} + \varepsilon\tilde{p} + \text{c.c.} \tag{1}$$

where $\varepsilon \ll 1$, and c.c. denotes the conjugate of the complex quantities $\tilde{u}_i$ and $\tilde{p}$. Linearizing around the basic flow, the equations for the perturbation quantities are obtained:

$$\frac{\bar{\mathrm{D}}\tilde{u}_i}{\mathrm{D}t} + \tilde{u}_j\frac{\partial\bar{u}_i}{\partial x_j} = -\frac{\partial\tilde{p}}{\partial x_i} + \frac{1}{Re}\frac{\partial^2\tilde{u}_i}{\partial x_j^2} \tag{2}$$

$$\frac{\partial\tilde{u}_i}{\partial x_i} = 0 \tag{3}$$

with

$$\frac{\bar{\mathrm{D}}}{\mathrm{D}t} = \frac{\partial}{\partial t} + \bar{u}_j\frac{\partial}{\partial x_j}$$

The boundary condition used for this system is $\tilde{u}_i = 0$ on the domain boundary.

A. Basic Flows

A detailed discussion of the numerical approach used to recover the basic states may be found elsewhere [7]; here, a brief summary is given. A Cartesian coordinate system is considered, taking $(x_1, x_2, x_3) \equiv (x, y, z)$ and $(u_1, u_2, u_3) \equiv (u, v, w)$. The basic flow is calculated by time-marching the vorticity transport equation:

$$\zeta_t + \bar{v}\zeta_y + \bar{w}\zeta_z - \frac{1}{Re}\nabla^2\zeta = 0 \tag{4}$$

where $\zeta = -\bar{w}_y + \bar{v}_z$ is the basic flow vorticity

$$\nabla^2 = \frac{\partial^2}{\partial y^2} + \frac{\partial^2}{\partial z^2}$$

and the stream function ψ is related with the vorticity through

$$\nabla^2\psi + \zeta = 0 \tag{5}$$

An equation analogous to Eq. (4) is solved for the axial component of velocity $\bar{u}$, which is decoupled from systems (4) and (5). Dimensional time t^* is nondimensionalized as

$$t = \frac{t^*\nu}{2\pi a_0^2} \tag{6}$$

The initial conditions for the flows analyzed are composed of an isolated or system of Lamb–Oseen vortices to which an axial flow has been superimposed. The initial vorticity $\zeta_0 = \zeta(t = 0)$ of a single such vortex is defined by

$$\zeta_0 = \frac{\Gamma_0}{\pi a_0^2}\, e^{-\frac{r^2}{a_0^2}} \tag{7}$$

where Γ is the circulation of the flow, defined by

$$\Gamma = \iint_{z>0} \zeta\,\mathrm{d}y\,\mathrm{d}z \tag{8}$$

Γ_0 is its initial value, and $a_0 = a(t = 0)$ is the initial vortex radius. Additionally, an initial axial velocity $\bar{u}_0 = \bar{u}(t = 0)$ and

$$\bar{u}(t = 0) = \bar{u}_0 = U_0 \exp\left[-\frac{r^2}{a_0^2}\right] \tag{9}$$

is defined, where U_0 is the peak value of the axial velocity; the latter is a free parameter measuring the jet strength [9,11]. The vortex radius $a = (a_y^2 + a_z^2)^{\frac{1}{2}}$ is based on the vorticity polar moment on the half-plane [12], where

$$\begin{aligned} a_y &= \left[\left(\iint_{z>0} \zeta(y - y_c)^2\,\mathrm{d}y\,\mathrm{d}z\right)\Big/\Gamma\right]^{\frac{1}{2}}, \\ a_z &= \left[\left(\iint_{z>0} \zeta(z - z_c)^2\,\mathrm{d}y\,\mathrm{d}z\right)\Big/\Gamma\right]^{\frac{1}{2}} \end{aligned} \tag{10}$$

and (y_c, z_c) denotes the position of the vorticity centroids

$$y_c = \frac{1}{\Gamma}\iint_{z>0} y\zeta\,\mathrm{d}y\,\mathrm{d}z, \qquad z_c = \frac{1}{\Gamma}\iint_{z>0} z\zeta\,\mathrm{d}y\,\mathrm{d}z \tag{11}$$

In the present case of a system of two vortices, the initial distance between the centroids is denoted by $b = 2z_c$. The flow Reynolds number is defined by

$$Re = \frac{\Gamma}{\nu} \tag{12}$$

where ν is the kinematic viscosity.

B. Numerical Solution of the Basic Flow Problem

An eigenvalue decomposition algorithm [4] is used to efficiently solve the Poisson equations arising from temporal discretization of Eq. (4) by the high-order algorithm proposed by Spalart et al. [13]. In contrast to the case discussed by Theofilis [4], periodic boundary conditions are used here, as justified by the disparity of the characteristic length scales of the vortex system and the much larger integration domain. This results in a particularly simple algorithm for the solution of the Poisson problems, as outlined next.

A typical Poisson problem to be solved during each fractional time step has the form

$$\nabla^2 f = g \tag{13}$$

defined in a rectangular domain

$$y \in [-y_\infty, y_\infty] \times z \in [-z_\infty, z_\infty]$$

The domain is discretized by N_y and N_z Fourier spectral-collocation points [14], whereby the corresponding collocation derivative matrices $\mathcal{D}_y^2$ and $\mathcal{D}_z^2$ denoting the second-order derivative with respect to the spatial variables y and z, respectively, have been used. Diagonalizing $\mathcal{D}_y^2 = A\kappa A^{-1}$ and $(\mathcal{D}_z^2)^T = B\lambda B^{-1}$, one obtains

$$A\kappa A^{-1} f + fB\lambda B^{-1} = g \tag{14}$$

$$(\kappa + \lambda)\hat{f} = \hat{g} \tag{15}$$

where $\hat{f} = A^{-1} f B$ and $\hat{g} = A^{-1} g B$. The system of algebraic Eq. (15) may be solved efficiently: that is, requiring $\mathcal{O}(N_y^2 + N_z^2)$ memory and $\mathcal{O}(N_y^3 + N_z^3)$ computing time for the forward and backward sweeps between (f, g) and $(\hat{f}, \hat{g})$ at each fractional time step, as opposed to $\mathcal{O}((N_y N_z)^2)$ memory and $\mathcal{O}((N_y N_z)^3)$ computing time that a direct solution of Eq. (13) would require.

C. Biglobal Eigenvalue Problem

The ansatz used to describe the small-amplitude perturbations is

$$\tilde{u}_i = \hat{u}_i(y, z) e^{i(\alpha x - \omega t)} \tag{16}$$

$$\tilde{p} = \hat{p}(y, z) e^{i(\alpha x - \omega t)} \tag{17}$$

where a temporal formulation has been adopted, considering that α is a real wave-number parameter associated with the axial periodicity length through $L_x = (2\pi/\alpha)$ and ω is the complex eigenvalue sought. Substitution into Eqs. (2) and (3) results in

$$i\alpha\hat{u} + \hat{v}_y + \hat{w}_z = 0 \tag{18}$$

$$\mathcal{L}\hat{u} - \bar{u}_y\hat{v} - \bar{u}_z\hat{w} - i\alpha\hat{p} = -i\omega\hat{u} \tag{19}$$

$$(\mathcal{L} - \bar{v}_y)\hat{v} - \bar{v}_z\hat{w} - \hat{p}_y = -i\omega\hat{v} \tag{20}$$

$$(\mathcal{L} - \bar{w}_z)\hat{w} - \bar{w}_y\hat{v} - \hat{p}_z = -i\omega\hat{w} \tag{21}$$

where

$$\mathcal{L} = 1/Re(-\alpha^2 + \partial^2/\partial y^2 + \partial^2/\partial z^2) - i\alpha\bar{u} - \bar{v}\partial/\partial y - \bar{w}\partial/\partial z$$

The complex generalized eigenvalue problem for the determination of ω may thus be obtained:

$$A\begin{pmatrix}\hat{u}\\ \hat{v}\\ \hat{w}\\ \hat{p}\end{pmatrix} = -i\omega B\begin{pmatrix}\hat{u}\\ \hat{v}\\ \hat{w}\\ \hat{p}\end{pmatrix} \tag{22}$$

D. Boundary Conditions for the EVP

Essential for the convergence of the serial numerical solution of the biglobal EVP on a shared-memory machine has been the exploitation in the eigenvalue problem of symmetries in the basic flow. Specifically, homogeneous symmetric and antisymmetric boundary conditions on the disturbance velocity components have been used to close this system. The use of symmetric/antisymmetric boundary conditions is justified because of the properties of system (22) in conjunction with the basic flow symmetries: $\bar{u}$ and $\bar{v}$ are symmetric about $z = 0$, whereas $\bar{w}$ is antisymmetric; mathematically expressed, the basic flow components satisfy

$$\bar{u}(y, z) = \bar{u}(y, -z)$$
$$\bar{v}(y, z) = \bar{v}(y, -z)$$
$$\bar{w}(y, z) = -\bar{w}(y, -z)$$

Analysis shows that if all eigenvalues are simple, the eigenfunctions necessarily have either an odd or an even z symmetry. More precisely, two combinations are possible:

1) The disturbance amplitude velocity components $\hat{u}$ and $\hat{v}$ are symmetric (Neumann boundary condition) about the plane $z = 0$, whereas $\hat{w}$ is antisymmetric (homogeneous Dirichlet boundary condition). This case follows the base flow structure, and the resulting instabilities are often referred to as *varicose* in the literature. The amplitude functions satisfy

$$\hat{u}(y, z) = \hat{u}(y, -z)$$
$$\hat{v}(y, z) = \hat{v}(y, -z)$$
$$\hat{w}(y, z) = -\hat{w}(y, -z)$$

2) The disturbance amplitude velocity components $\hat{u}$ and $\hat{v}$ are antisymmetric (homogeneous Dirichlet boundary condition) about the plane $z = 0$, alongside a $\hat{w}$, which is symmetric (Neumann boundary condition). This case is referred to as *sinuous* instabilities. Here,

$$\hat{u}(y, z) = -\hat{u}(y, -z)$$
$$\hat{v}(y, z) = -\hat{v}(y, -z)$$
$$\hat{w}(y, z) = \hat{w}(y, -z)$$

holds for the amplitude functions at the plane of symmetry.

Using the preceding symmetries permits reducing the size of system (22) by considering only half of the spanwise domain; this halves the memory requirements, and the computing time is also reduced in line with the cost of the algorithm used for the recovery of the eigenspectrum.

E. Numerical Solution of the EVP

From a linear-stability-analysis point of view, the most important eigenvalues are those closest to the axis $\omega_i = 0$ and an iterative method has been used here for their determination. Specifically, the Arnoldi algorithm, well-established in biglobal linear-instability problems [4], has been used. Because the eigenvalues closest to the imaginary axis are sought, a simple transformation of the original eigenvalue problem (22) is used to convert the original problem into one in which the desired values have large modules. Note that the eigenvectors are not affected by this transformation. Specifically, the problem

$$A^{-1}B\Phi = \mu\Phi, \qquad A^{-1}B = C, \qquad C\Phi = \mu\Phi \tag{23}$$

is solved, where Φ is the vector of unknowns shown in Eq. (22). This transformation converts the original generalized into the standard EVP. A finite but small (compared with the leading dimension of A and B) number of eigenvalues (equal to the Krylov subspace dimension) m are sought, which are obtained by application of the Arnoldi algorithm.

In both the isolated Batchelor-vortex validation case and the dipole analyses that follow, the spatial discretization of Eq. (22) is performed using nodal mixed finite elements of the Taylor–Hood type. The mixed interpolation for the velocity and pressure eigenfunctions can be expressed as

$$\hat{u}_i = \psi_\alpha \hat{u}_i^\alpha \qquad (\alpha = 1, \ldots, N) \tag{24}$$

$$\hat{p} = \psi_\lambda \hat{p}^\lambda \qquad (\lambda = 1, \ldots, \mathrm{NL}) \tag{25}$$

where N and NL are the number of quadratic and linear nodes used

for the discretization of the velocity and pressure, respectively. Nodal points are chosen beforehand and the Lagrange basis has the notable property that $\Phi_p(x_q) = \delta_{pq}$, where δ_{pq} represents the Kronecker delta. This property implies that the approximate solution in a nodal point x_q can be calculated as

$$u(x_q) = \sum_{p=0}^{P} \hat{u}_p \Phi_p^B(x_q) = \sum_{p=0}^{P} \hat{u}_p \delta_{pq} = \hat{u}_q \tag{26}$$

where the expansion coefficient $\hat{u}_p$ can be defined in terms of the approximate solution at the point/node x_q. The coefficients therefore have a physical interpretation and they represent the approximate solution at the points x_q. In this way, Lagrange expansion basis is a typical example of nodal expansion.

III. Results

A. Basic Flow

A system of two counter-rotating vortices has been defined by the parameters $a(t=0) = 0.25$ and $b_0 = b(t=0) = 1/0.134$. A wide square integration domain has been taken, the extent of which, L, is taken to fulfill $L \gg b_0$, such that the periodic boundary conditions do not affect the results of the simulations. The equations of motion (4) and (5) have been integrated in time until certain predetermined criteria, indicated next, are met. Resolutions upward of $N_y = Nz = 400$ Fourier collocation points per spatial direction have been used, and integral quantities, as defined previously, have been monitored throughout the simulation. In the multiparametric problem at hand, a constant initial circulation of unity has always been considered, whereas basic flows have been run for two Reynolds number values ($Re = 3.180 \times 10^3$ and 5×10^3) and three initial axial velocity values ($U_0 = 0.5/\pi, 0.75/\pi$, and $1/\pi$), whereas basic flows were extracted from the DNS results analyzed at three distinct times, as discussed in what follows.

Figure 1 shows the dependence of y_c on time; the constant slope of the curve obtained indicates the constant descent velocity of the vortex system; three time instances are marked on this figure and will be defined in what follows. The vortex aspect ratio $E = a_z/a_y$, shown in Fig. 2, settles to a linear growth after a short initial transient, the latter indicating the short period during which the initially imposed analytical vorticity distribution adjusts itself to the

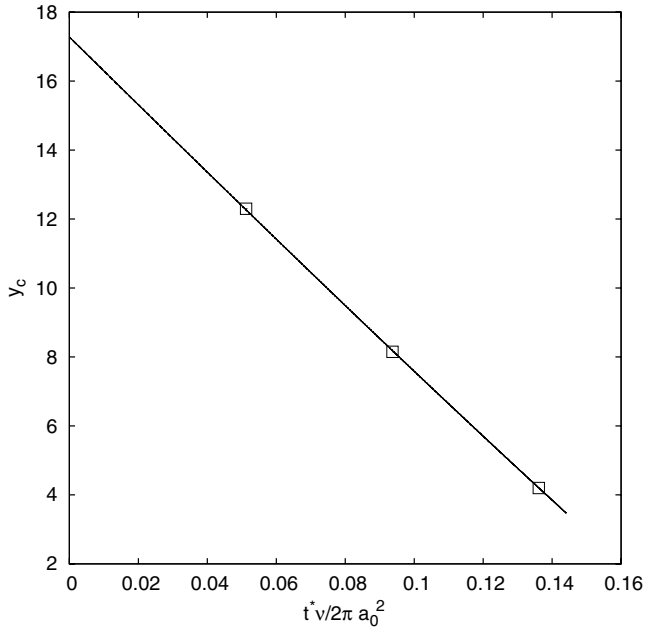

Fig. 1 Dependence of y_c on nondimensional time $t^*\nu/2\pi a_0^2$; the system of counter-rotating vortices descends by the constant velocity dy_c/dt; $Re = 3180$ and $U_0 = 0.5/\pi$; also shown are the three time instants ($t_0 - \Delta t$, t_0, and $t_0 + \Delta t$) at which analyses have been performed; the corresponding basic flows may be seen in Fig. 5.

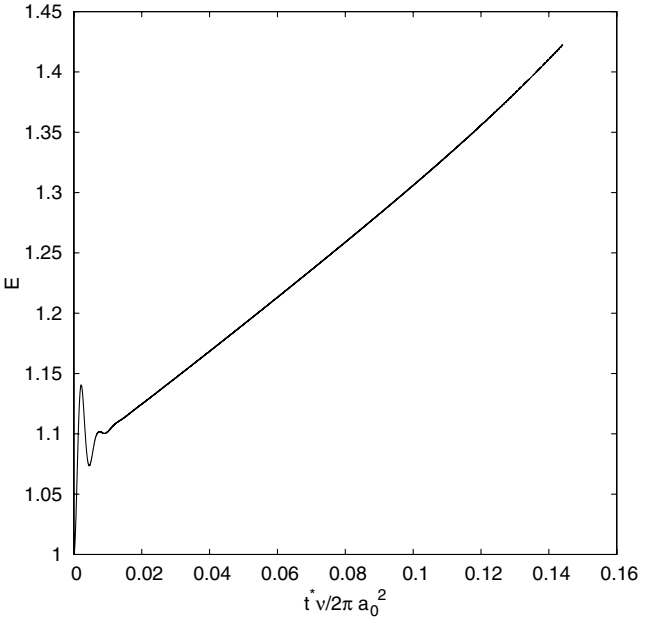

Fig. 2 A long-time linear dependence of the vortex aspect ratio $E = a_z/a_y$ on time, as recovered from the 2-D DNS; $Re = 3180$ and $U_0 = 0.5/\pi$.

equations of motion. The rather close agreement of the vortex radius a, as obtained by the DNS and as predicted by the theoretical curve

$$a_{\text{th}} = a_0\left(1 + \frac{4\nu t}{a_0^2}\right)^{\frac{1}{2}}$$

is shown in Fig. 3. This result also shows the low degree of interaction between the two vortices at this set of parameters. Figure 4 shows the dependence of the dipole aspect ratio a/b on time. Stopping the simulations when this ratio reaches the value $a/b = 1/4$ defines one time, $t_0 \approx 0.09369$, at which one of the subsequent instability analyses was performed. Instability-analysis results obtained at this time have been compared with those corresponding to two other time instants: at equal nondimensional distance $\Delta t \approx 0.04244$ before and subsequent to t_0 identified in Fig. 1 and,

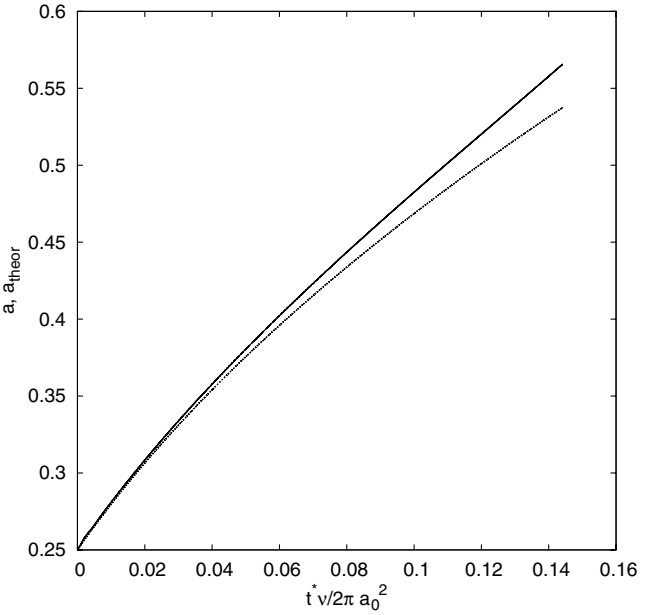

Fig. 3 Comparison of the vortex radius a obtained in the DNS (solid line) against the theoretical value $a_{\text{th}} = a_0(1 + (4\nu t/a_0^2))^{\frac{1}{2}}$ (dashed line), indicating weak interaction of the vortices; $Re = 3180$ and $U_0 = 0.5/\pi$.

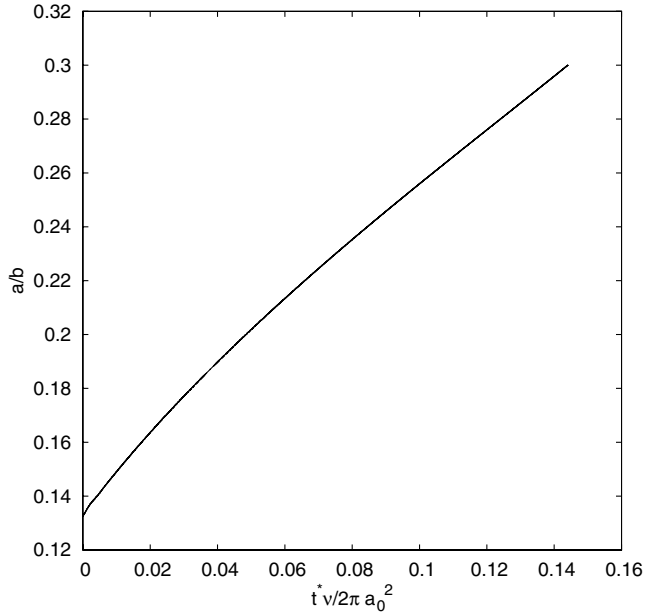

Fig. 4 Dependence of the dipole aspect ratio a/b on time; basic flows to be analyzed are extracted at a time such that $a/b = 0.25$; $Re = 3180$ and $U_0 = 0.5/\pi$.

respectively, denoted as $t_0 - \Delta t$ and $t_0 + \Delta t$ in Fig. 5. The viscous diffusion of the basic state is clearly seen in these results. By the end of the simulation, it has been verified that the circulation is constant to within 2×10^{-3}.

B. Instability Analyses

Before analyzing the system of vortices obtained in the previous section, it is instructive to present results obtained in the well-studied Batchelor-vortex instability problem [10]. The second-order FEM method discussed by González et al. [6] is employed on this analytically constructed basic flow, and the resulting system is solved in a large domain of 80 Batchelor-vortex radii, such that homogeneous Dirichlet boundary conditions may be imposed on all amplitude functions at the boundary of the domain. Although the classic instability analysis that exploits periodicity in the azimuthal direction [10] could have been used in this limiting case, the biglobal EVP [Eqs. (18–21)] has been solved without the need to resort to this assumption.

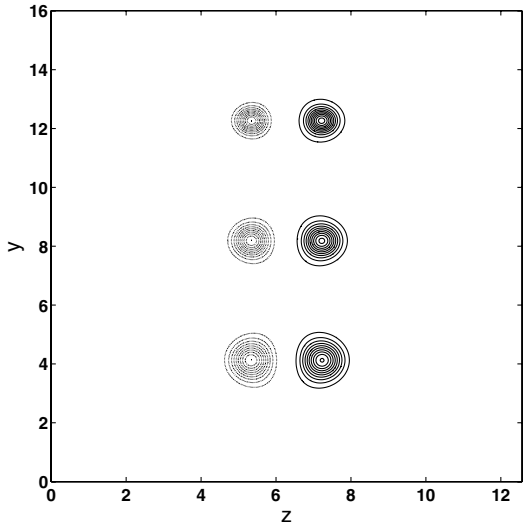

Fig. 5 Photographs of three basic states analyzed, as obtained by the 2-D DNS at times $t = t_0 - \Delta t$ (upper), $t = t_0$ (middle), and $t = t_0 + \Delta t$ (lower); $Re = 3180$ and $U_0 = 0.5/\pi$.

Table 1 Eigenvalues of the single Batchelor vortex, calculated on 84,121 nodes by the second-order FEM

Mayer–Powell [10]			FEM	
Re	α	ω_i	ω_i	ω_r
40	0.436	1.06×10^{-2}	1.057×10^{-2}	0.0150
100	0.418	9.61×10^{-3}	9.609×10^{-3}	2.8356

Results at two combinations of the Reynolds number and axial-wave-number parameters are shown in Table 1. Two conclusions may be drawn: On one hand, the (low-order) FEM is capable of delivering accurate results in a manner analogous to that demonstrated in the flows to which it was previously applied [6]. On the other hand, the mesh required for such results to be obtained is prohibitively large: $\mathcal{O}(8 \times 10^4)$ nodes were used to resolve the cases presented, resulting in typical in-core memory for the storage of the discretized matrix of $\mathcal{O}(4$ GB) and corresponding runtime demanded by the Arnoldi algorithm of $\mathcal{O}(10)$ CPU hours on a 3 GHz Intel P-IV PC. To mitigate the memory requirements, a hybrid FEM calculation mesh, shown in the Fig. 6, has been used. In the vicinity of the basic flow vortex, this mesh comprises a finely resolved structured core of one dimension (in radius units) embedded

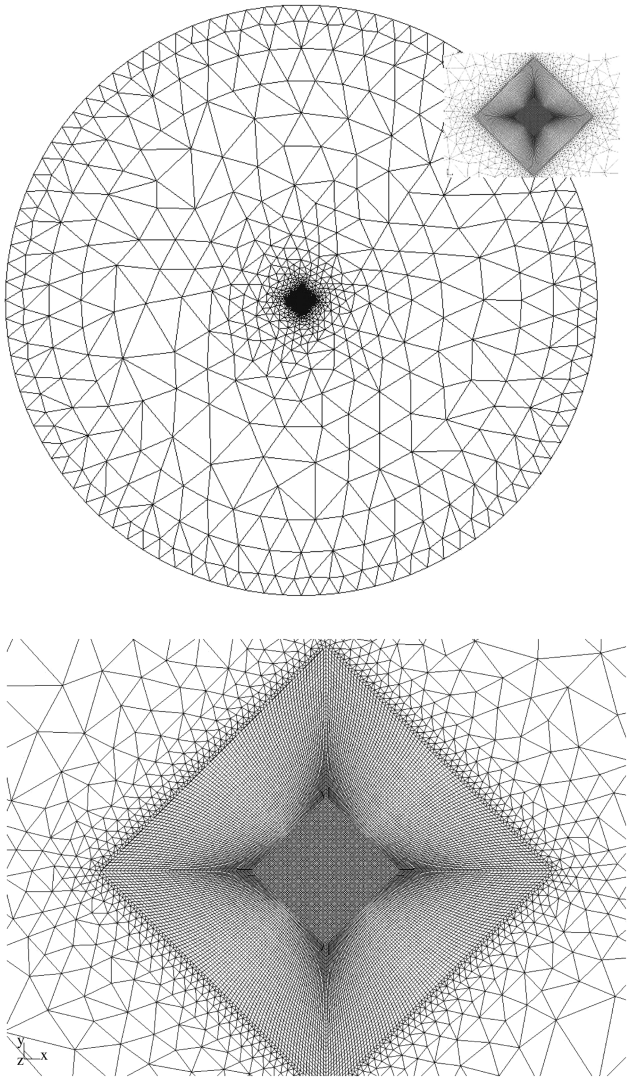

Fig. 6 Hybrid FEM mesh used for low-order biglobal instability analysis of the isolated Batchelor-vortex problem (the radius of the image is of the order of 80 vortex radii; also shown is a detail of the mesh around the vortex core of dimension unity) (upper) and b) corresponding to the vortex core, amplified for clarity (lower).

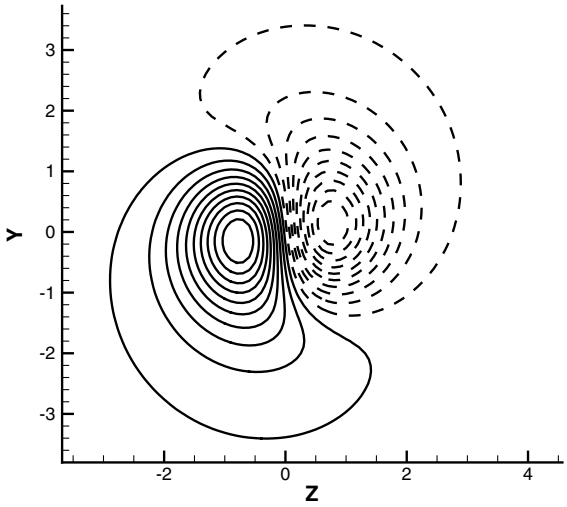

Fig. 7 Amplitude function of the normalized axial perturbation $\hat{u}$ in the Batchelor vortex at $Re = 40$ and $\alpha = 0.436$ obtained through numerical solution of Eqs. (18–21).

into an unstructured mesh, the density of which decreases monotonically to the end of the calculation domain.

The extent of the domain is calculated on the basis of the following considerations: although the vortex core radius is of order 2π, homogeneous Dirichlet boundary conditions are imposed in the far field. As identified by Delbende et al. [11], the amplitude functions of the perturbation components are expected to decay exponentially as $r \to \infty$ according to $e^{-\alpha r}$. In this respect, the far-field boundaries must be situated sufficiently far away from the vortex core, especially for small α values, for the error that the Dirichlet boundary condition induces to be negligible. The axial disturbance velocity component $\hat{u}$ of a Batchelor vortex at $Re = 40$ and $\alpha = 0.436$ is shown in Fig. 7; the characteristic dimension of this structure, which can be identified as mode $m = 1$ in a local analysis context, is of order unity.

Table 2 Set of meshes used for the numerical convergence ($Re = 3180$, $\alpha = 3.0$, and $U_0 = 0.5/\pi$)

No. nodes	Symmetry	$10^2 \times \omega_i$	$10^2 \times \omega_r$	CPU time, s
49,621	No	−4.597	−6.076	1575
61,553	No	−4.598	−6.069	1738
51,229	Yes	−4.603	−6.072	1644
69,687	Yes	−4.603	−6.072	1925

Based on this experience, analogous FEM grids have been calculated for the biglobal instability analysis of the dipole. Again, the extent of the domain is the square $x, y \in [-40, 40]$, as seen in Fig. 8. However, the innermost structured grid of the highest resolution has been embedded into a second structured grid of lower density before the system has blended into the unstructured mesh away from the location of the vortices. An analogous meshing strategy has been followed successfully in the recent spectral-hp-element analysis of Batchelor vortices by Broadhurst and Sherwin [15]. In addition, symmetries have been imposed in the present work, as explained in Sec. II, to halve the storage necessary for the discretization of the biglobal EVP. Concretely, the memory requirements for the dipole analysis on the mesh of Fig. 8 are below 4 GB, as opposed to double that amount, which would have been necessary had symmetries not been imposed. This has the

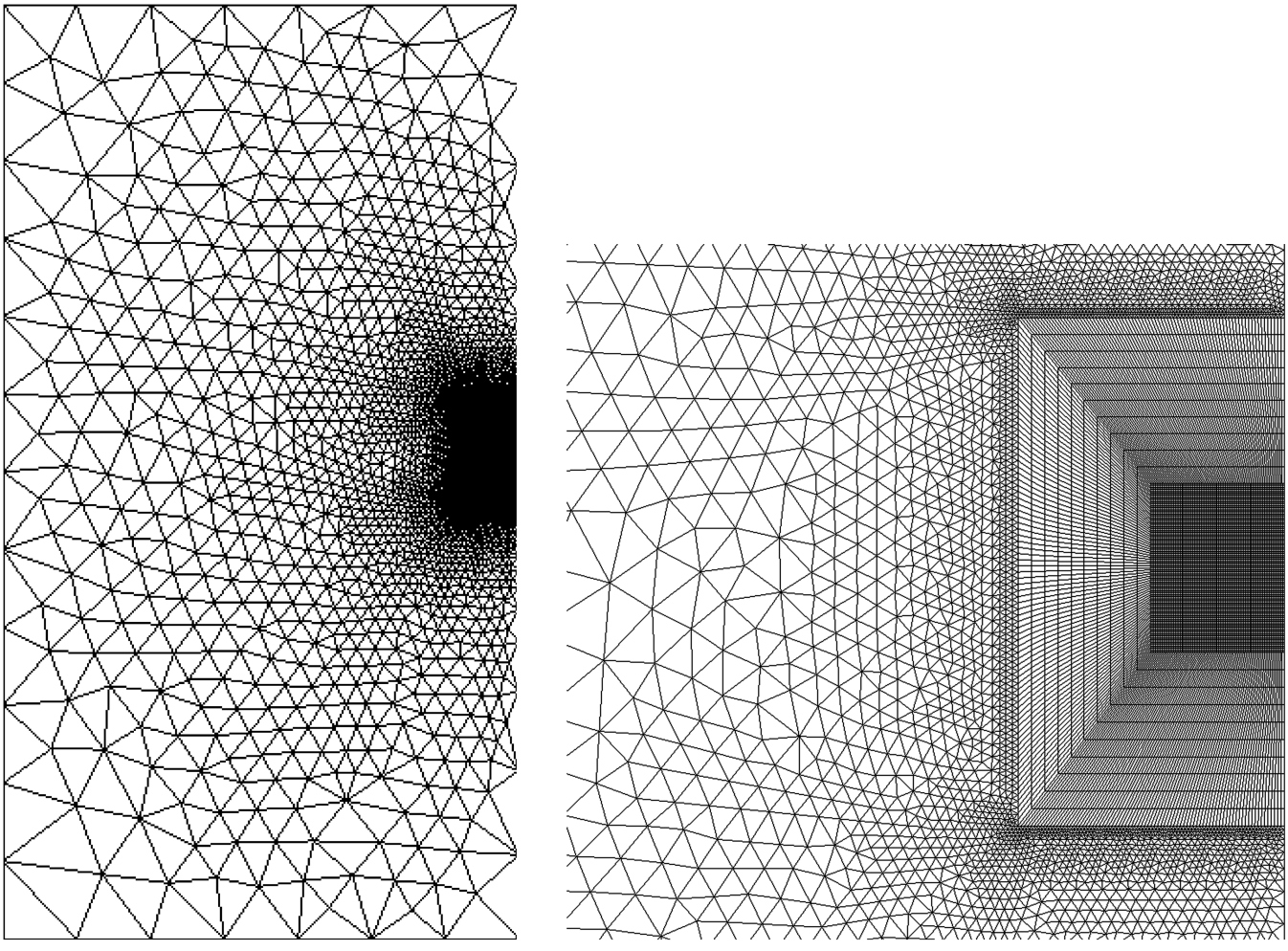

Fig. 8 Global view of the mesh used for the dipole vortex analysis (left) and different levels of detail of this mesh (right).

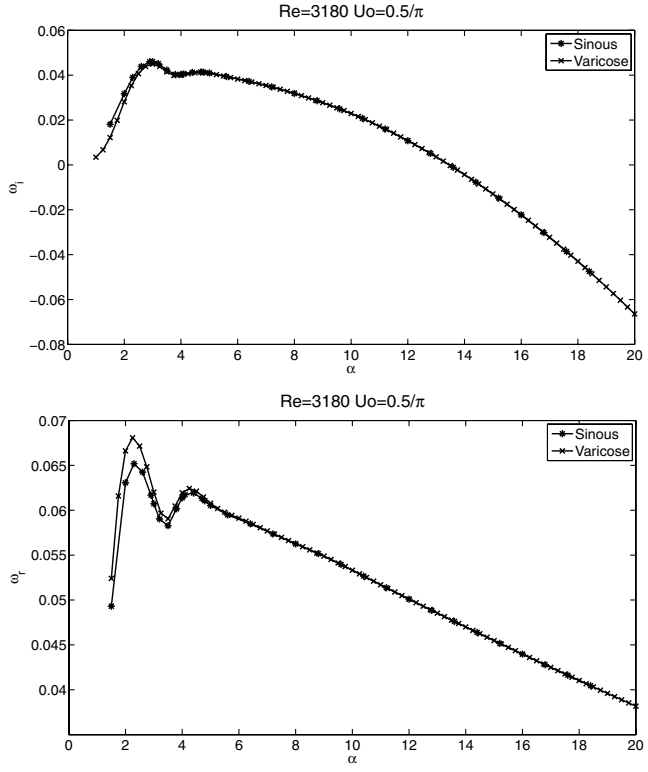

Fig. 9 Comparison between the amplification rates (upper) and frequencies (lower) of the leading two eigenmodes corresponding to sinuous and varicose boundary conditions at $Re = 3180$ and $U_0 = 0.5/\pi$.

consequence that analyses may be performed on a PC as opposed to a larger shared-memory machine.

The convergence history at a specific set of parameters, typical of that obtained at all parameter values examined, is shown in Table 2. Shown are the leading eigenvalues when symmetries are imposed, and the results are compared with those on different meshes when symmetries are not exploited. In all instability results obtained, it has been observed that the eigenmodes of the sinuous and varicose modes were very close to each other, whereas the amplitude functions were different, each corresponding to the symmetries imposed.

The frequencies of the leading two pairs of unstable eigenmodes (sinuous and varicose) in the axial-wave-number parameter range $\alpha \in [1, 20]$ at a specific set of parameters ($Re = 3180$ and $U_0 = 0.5/\pi$) are shown in Fig. 9. Two relative maxima in the amplification rates of the two modes may be identified at $\alpha \approx 3$ and 5 (there is indication of a mode-splitting at $\alpha \approx 4$), whereas the dependence of both the frequency and the amplification rate of the two modes on the axial wave number is quite similar.

Two interesting axial-wave-number limits may be discussed: First, $\alpha_s \approx 13.6$ (i.e., for axial periodicity lengths $L_x = 2\pi/\alpha_s \leq 0.46$), beyond which only flows that are stable against all three-dimensional perturbations may be expected. At the other wave-number-range extreme, it should be noted that the appearance of the term α^2/Re in the biglobal EVP renders obtaining accurate numerical solutions increasingly more challenging as $\alpha \to 0$ ($L_x \to \infty$). Nevertheless, the situation appears to be qualitatively different from that in the short-axial-wave-number range; no indication of stabilization of the flow against three-dimensional long-axial-wave-number perturbations could be obtained. Given the practical equality of the eigenmode results for the two classes of

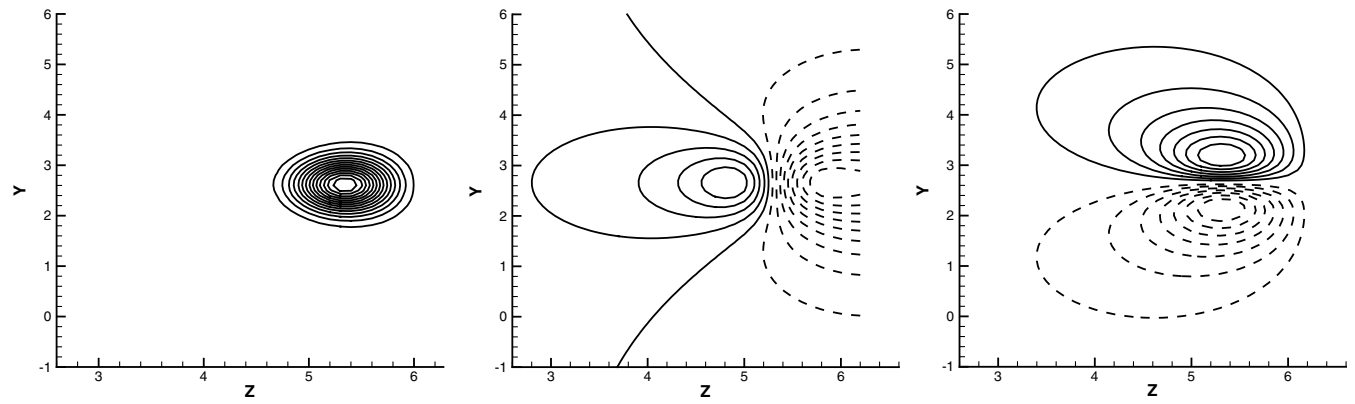

Fig. 10 Base flow velocity $(\bar{u}, \bar{v}, \bar{w})^T$ at $Re = 3180$, $U_0 = 0.5/\pi$, $\alpha = 3.0$. Half-plane representation. Fourteen equally spaced isolines between the respective maxima $\hat{u}(0.046, 0)$, $\hat{v}(0.165, -0.333)$, and $\hat{w}(0.192, -0.192)$.

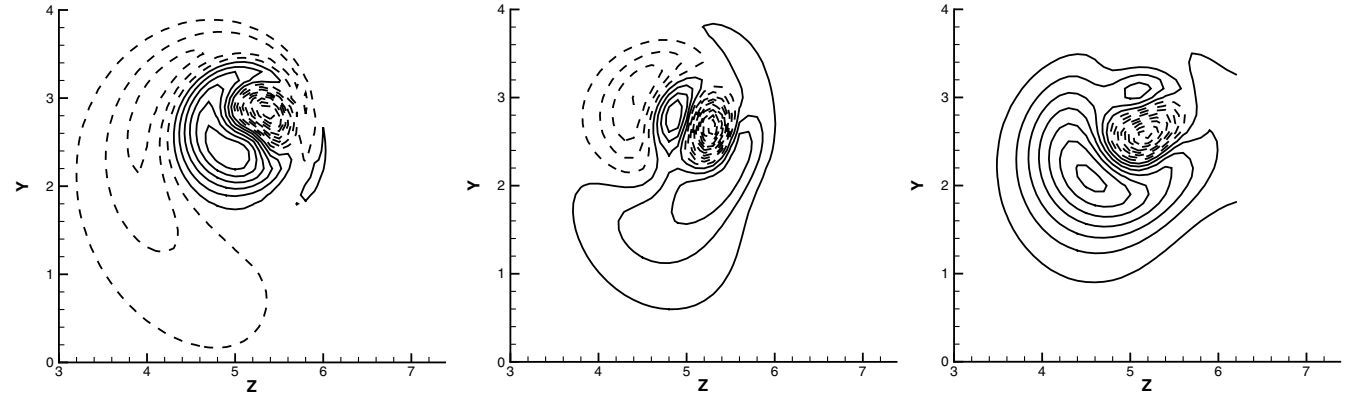

Fig. 11 Half-plane representation of amplitude functions $(\hat{u}, \hat{v}, \hat{w})^T$ of the leading eigenmode at $Re = 3180$, $U_0 = 0.5/\pi$ and $\alpha = 3.0$ obtained through numerical solution of Eqs. (18–21) with 15 equally spaced isolines between the respective maxima $\hat{u}(0.587, -0.783)$, $\hat{v}(0.393, -1)$, and $\hat{w}(0.625, -0.625)$.

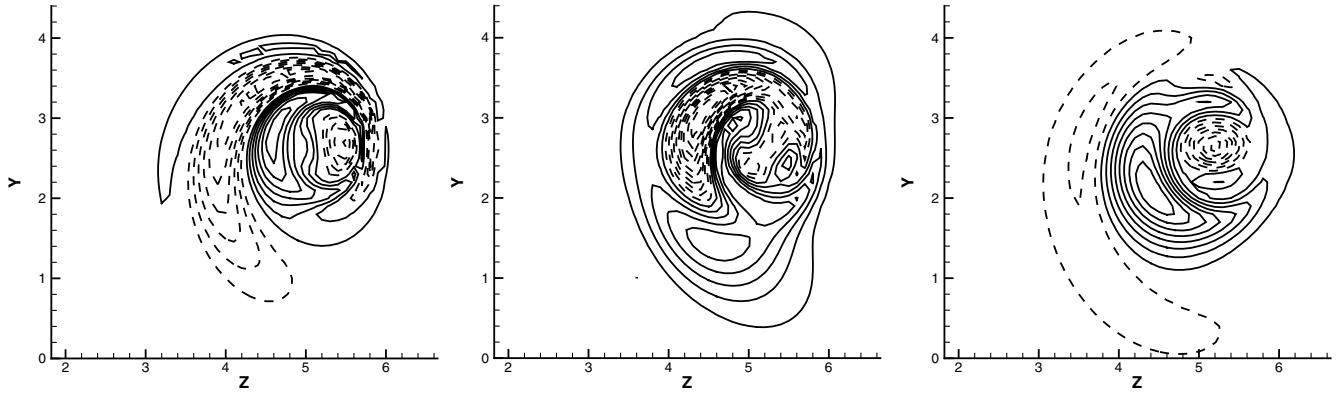

Fig. 12 Half-plane representation of amplitude functions $(\hat{u}, \hat{v}, \hat{w})^T$ of the second mode at $Re = 3180, U_0 = 0.5/\pi, \alpha = 3.0$, obtained through numerical solution of Eqs. (18–21) with 15 equally spaced isolines between the maxima $\hat{u}(0.876, -0.877)$, $\hat{v}(0.309, -0.612)$, and $\hat{w}(1, -0.760)$.

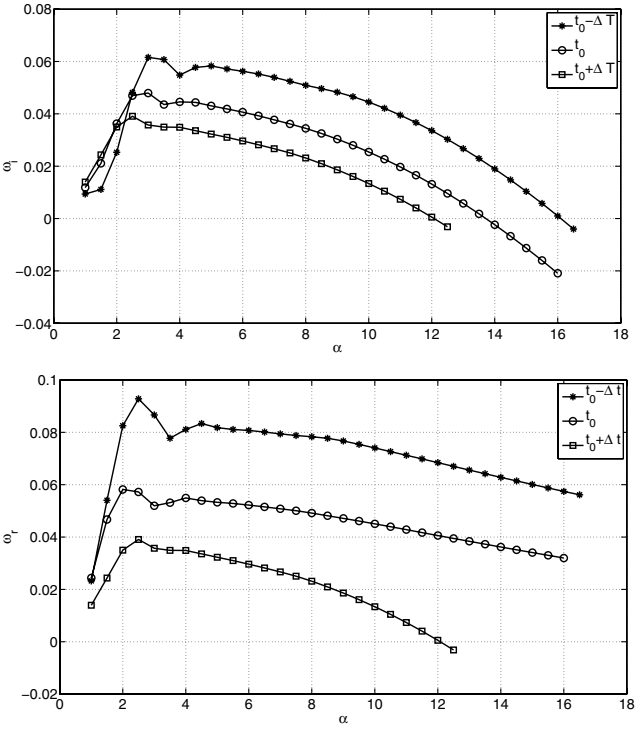

Fig. 13 Dependence of amplification rate (upper) and frequency (lower) of the most unstable mode on time, at constant $Re = 3180$ and initial axial flow velocity; $U_0 = 0.75/\pi$.

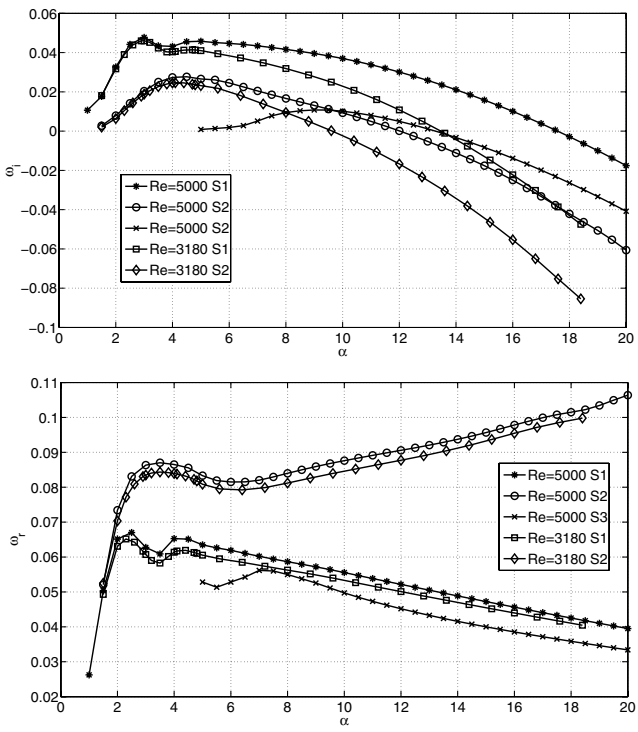

Fig. 14 Dependence of amplification rates (upper) and frequencies (lower) on Reynolds number, at constant initial value of the axial flow velocity $U_0 = 0.5/\pi$ and time t_0.

symmetries imposed and in the interests of clarity of presentation, results of the sinuous modes alone will be presented in what follows.

The basic flow components $\bar{u}$, $\bar{v}$, and $\bar{w}$ at $Re = 3180$ and $0.5/\pi$ are shown in Fig. 10. The corresponding disturbance amplitude functions $\hat{u}$, $\hat{v}$, and $\hat{w}$ at $\alpha = 3.0$ pertaining to the leading and the second most unstable modes are shown in Figs. 11 and 12, respectively. A key observation in these and all other results obtained (but not shown here) is that the spatial inhomogeneity of the amplitude functions along the azimuthal direction may be appreciated. Features of the eigenmodes, known from classic instability analyses that invoke azimuthal homogeneity as an assumption, may be seen in these results. Specifically, remnants of elliptic instability in the vortex core are visible. However, there is no symmetry in the corresponding lobe structures, which would make an attempt to recover these eigenmodes by imposition of azimuthal homogeneity erroneous. Even more significantly, the braids surrounding the vortex core are essential parts of the amplitude functions of the same (or larger) magnitude as the structures in the vortex cores. Such structures are clearly out of reach of instability approaches invoking periodicity along the azimuthal direction; use of the biglobal instability concept is mandatory for their recovery.

Analyses have been performed that monitor the instability of basic flow photographs extracted from the 2-D DNS at different times. The full range of axial-wave-number parameters previously found to correspond to unstable perturbations have been monitored at constant values of the Reynolds number ($Re = 3180$) and initial axial velocity parameter ($U_0 = 0.75/\pi$). The eigenmodes of the basic flows shown in Fig. 5 are shown in Fig. 13. The amplification rates demonstrate that the progressive diffusion of the basic state results in stabilization of the flow. The wavelength corresponding to the maximally amplified mode is approximately constant, whereas the frequency decreases as time increases.

Turning to the dependence of the unstable eigenspectrum on Reynolds number changes at constant t_0 and $U_0 = 0.5/\pi$ values, Fig. 14 shows amplification rate and frequency results of analyses at $Re = 3180$ and 5000. Qualitatively analogous conclusions with those at $Re = 3180$ may be drawn at the higher Reynolds number value, as far as the leading eigenmodes are concerned. Again, the dependence on α of the amplification rates of the sinuous and varicose modes follows one another closely; consequently, only the most unstable sinuous modes, denoted as S, are shown in this figure. Interestingly, compared with the results at $Re = 3180$, at this

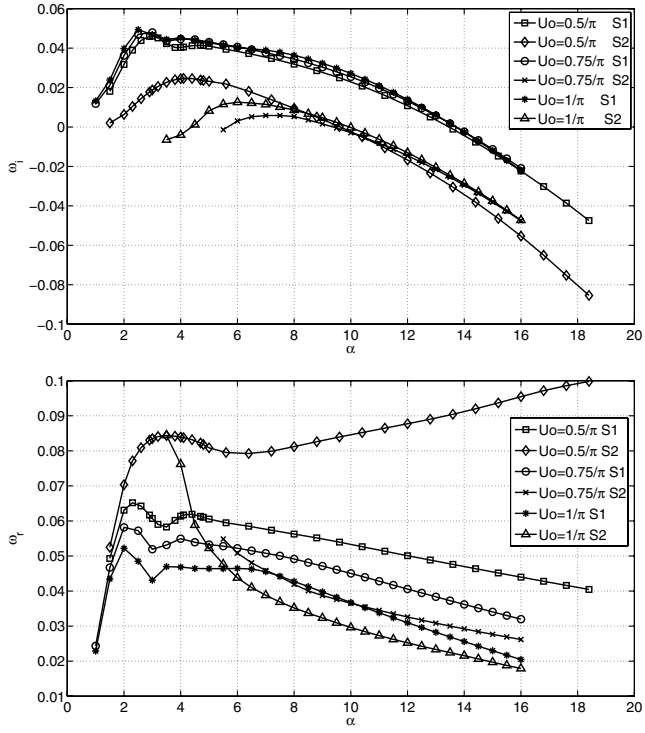

Fig. 15 Dependence of amplification rates (upper) and frequencies (lower) on the initial axial flow parameter value U_0 at constant Reynolds number $Re = 3180$ and time t_0.

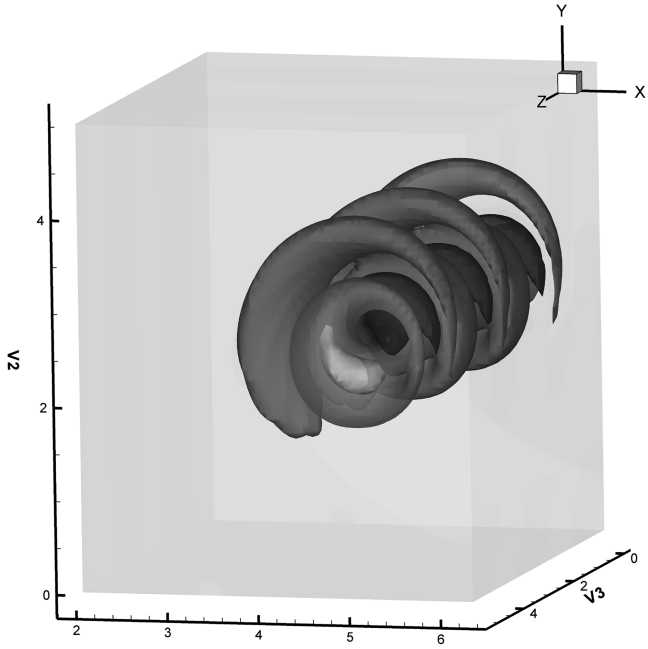

Fig. 16 Superposition upon the steady laminar basic state at $Re = 3180$, $U_0 = 0.5/\pi$, of its most amplified biglobal eigenmode at amplitude 1%. Axial spatial direction reconstructed using $L_x = 2\pi/\alpha$, with $\alpha = 3.0$; eigenvalue $\omega_i = 0.04603$, $\omega_r = 0.06072$.

Reynolds number value, an additional mode $S3$, which peaks at $\alpha \approx 8$, is amplified at $Re = 5000$. However, the growth rate of the new mode remains lower than those of the modes $S1$ and $S2$, discovered at $Re = 3180$ and also present at $Re = 5000$.

Finally, the effect on the eigenspectrum of changes in the initial value of the axial velocity parameter U_0 at constant $Re = 3180$ and time t_0 is shown in Fig. 15. Three values of U_0 ($0.5/\pi$, $0.75/\pi$, and $1/\pi$) have been examined, and it may be seen that the amplification rate of the leading eigenmode $S1$ increases very slightly with an increase in this parameter. In contrast, the amplification rate of mode $S2$ is strongly diminished by an increase in the U_0 parameter, whereas the peak amplification shifts toward higher α (lower axial periodicity wavelengths). Nevertheless, the $\Im\{\omega\}$ values of the second unstable mode are substantially lower than those of $S1$, and so the key message from this experimentation is that the initial value of the axial velocity hardly affects the instability characteristics of the leading eigenmode. To a lesser extent, the same statement holds for the frequencies of the leading eigenmode, although there is a mild decrease in these quantities when U_0 increases.

Finally, a linear superposition of the leading eigenmodes upon the basic state at $Re = 3180$ produces the structure shown in Fig. 16. Such structures, qualitatively known from DNS and experiments, may well be confused with nonlinear phenomena; the present analysis is the first of its kind to demonstrate that their origin is a linear (albeit biglobal) modal mechanism.

IV. Conclusions

A spectrally accurate two-dimensional DNS methodology has been used to obtain the time evolution of a pair of counter-rotating vortices, the initialization of which used the Batchelor model. Photographs of this flowfield, corresponding to different times, were considered as quasi-steady basic states and were analyzed with respect to their instability against three-dimensional axially periodic disturbances. The biglobal-analysis context employed permitted relaxing the assumption of azimuthal homogeneity that was invariably used in earlier analyses of problems of this class. The spatial structure of the (two-dimensional) amplitude functions of the eigenmodes obtained provide a posteriori justification for the use of the biglobal concept.

From a numerical point of view, what has become clear by the present work is that the Taylor–Hood FEM, as applied to the biglobal EVP solution [6], can only provide reliable results when appropriate calculation meshes have been designed. The resolution requirements of the latter become prohibitively high for serial in-core solutions of the EVP, such that the method quickly loses its competitive advantage of geometric flexibility. To mitigate the computational demands resulting from the second-order FEM formulation, a high-order FEM version of the biglobal EVP solver for the study of problems of this class is currently under development; first results on closed flows have been shown elsewhere [16].

From a physical point of view, it is clear that only a small set of characteristic parameter values may be examined in the present multiparametric problem, each addressing a different aspect of the dipole instability. Here, the Reynolds number, the initial strength of the axial velocity of the dipole, and different times along the evolution of the dipole, corresponding to different degrees of its diffusion, have been examined. In all cases, the full range of unstable axial-wave-number parameters has been identified for the first time, and a consistent picture of the instability of the dipole has emerged. The Reynolds number and initial peak axial velocity were found to have a minor effect on the peak amplification rates, although they do affect the leading eigenmodes at off-peak conditions in a systematic manner. On the other hand, the viscous decay of the dipole with the passing of time results in an flow that is increasingly more stable against all three-dimensional perturbations.

In addition to studying the instability of the flow at more values of the parameters examined here, a major future extension of the present work could be devoted to repeating the entire set of computations presented here in analyses at different values of the initial distance between the vortex cores. This endeavor is expected to be significantly facilitated by the aforementioned high-order FEM methods, and its results will be presented in due course.

Acknowledgments

The material is based upon work partially sponsored by contract numbers AST4-CT-2005-012338 (European Union Specific Targeted Research Project: Far Wake) and TRA2005-08983/TAIR

(Ministerio de Educación y Ciencia, Plan Nacional de Investigación).

References

[1] Winckelmans, G., and Leonard, A., "Contributions to Vortex Particle Methods for the Computation of Three-Dimensional Incompressible Unsteady Flows," *Journal of Computational Physics*, Vol. 109, No. 2, 1993, pp. 247–273. doi:10.1006/jcph.1993.1216

[2] Hein, S., and Theofilis, V., "On Instability Characteristics of Isolated Vortices and Models of Trailing-Vortex Systems," *Computers and Fluids*, Vol. 33, Nos. 5–6, 2004, pp. 741–753. doi:10.1016/j.compfluid.2003.05.004

[3] Jacquin, L., Fabre, D., Sipp, D., Theolis, V., and Vollmers, H., "Instability and Unsteadiness of Aircraft Wake Vortices," *Aerospace Science and Technology*, Vol. 7, No. 8, 2003, pp. 577–593. doi:10.1016/j.ast.2003.06.001

[4] Theofilis, V., "Advances in Global Linear Instability Analysis of Nonparallel and Three-Dimensional Flows," *Progress in Aerospace Sciences*, Vol. 39, No. 4, 2003, pp. 249–315. doi:10.1016/S0376-0421(02)00030-1

[5] Broadhurst, M., Theofilis, V., and Sherwin, S. J., "Spectral Element Stability Analysis of Vortical Flows," 6th IUTAM Laminar-Turbulent Transition Symposium, Bangalore, India, International Union of Theoretical and Applied Mechanics Paper 2006-2877, 2006, pp. 153–158.

[6] González, L. M., Theofilis, V., and Gomez-Blanco, R., "Finite Element Numerical Methods for Viscous Incompressible Biglobal Linear Instability Analysis on Unstructured Meshes," *AIAA Journal*, Vol. 45, No. 4, 2007, pp. 840–855. doi:10.2514/1.25410

[7] Theofilis, V., "Direct Numerical Simulation of the Roll-Up Process of a Trailing-Vortex System, Using Experimentally Obtained Data at Realistic Reynolds Numbers," DLR, German Aerospace Center, TR IB-224-2002-C-12, Goettingen, Germany, 2002.

[8] Capart, R., and Winckelmans, G., "On Characterization of the Rollup Produced by Different Span Loadings," Univ. Catholique de Louvain, TR AW-UCL-111-002D, Louvain, Belgium, 2002.

[9] Lacaze, L., Ryan, K., and Le Dizes, S., "Elliptic Instability in a Strained Batchelor Vortex," *Journal of Fluid Mechanics*, Vol. 577, 2007, pp. 341–361. doi:10.1017/S0022112007004879

[10] Mayer, E. W., and Powell, K. G., "Viscous and Inviscid Instabilities of a Trailing Vortex," *Journal of Fluid Mechanics*, Vol. 245, 1992, pp. 91–114. doi:10.1017/S0022112092000363

[11] Delbende, I., Chomaz, J.-M., and Huerre, P., "Absolute/Convective Instabilities in a Batchelor Vortex: A Numerical Study of the Linear Response," *Journal of Fluid Mechanics*, Vol. 355, 1998, pp. 229–254. doi:10.1017/S0022112097007787

[12] Sipp, D., Jacquin, L., and Cosssu, C., "Self-Adaptation and Viscous Selection in Concentrated Two- Dimensional Vortex Dipoles," *Physics of Fluids*, Vol. 12, No. 2, 2000, pp. 245–248. doi:10.1063/1.870325

[13] Spalart, P. R., Moser, R. D., and Rogers, M. M., "Spectral Methods for the Navier–Stokes Equations with One Infinite and Two Periodic Directions," *Journal of Computational Physics*, Vol. 96, No. 2, 1991, pp. 297–311. doi:10.1016/0021-9991(91)90238-G

[14] Canuto, C., Hussaini, M. Y., Quarteroni, A., and Zang, T. A., *Spectral Methods: Fundamentals in Single Domains*, Springer, New York, 2006.

[15] Broadhurst, M., and Sherwin, S. J., "The Role of Helical Instabilities in Initiating Asymmetric Break-Down of a Batchelor Vortex," *Journal of Fluid Mechanics* (submitted for publication).

[16] González, L. M., de Vicente, J., and Theofilis, V., "High-Order Finite Element Methods for Global Viscous Linear Instability Analysis of Internal Flows," 18th AIAA Computational Fluid Dynamics Conference, Miami, FL, AIAA Paper 2007-3840, June 2007.

A. Tumin
Associate Editor